

# Probe of unparticles at the LHC in exclusive two lepton and two photon production via photon-photon fusion

İ. Şahin\*

*Department of Physics, Zonguldak Karaelmas University, 67100 Zonguldak, Turkey*

S. C. İnan†

*Department of Physics, Faculty of Sciences,*

*Ankara University, 06100 Tandogan, Ankara, Turkey and*

*Department of Physics, Cumhuriyet University, 58140 Sivas, Turkey*

## Abstract

The exclusive production  $pp \rightarrow pXp$  is known to be one of the most clean channels at the LHC. We investigate the potential of processes  $pp \rightarrow p\ell^-\ell^+p$  and  $pp \rightarrow p\gamma\gamma p$  to probe scalar and tensor unparticles by considering three different forward detector acceptances;  $0.0015 < \xi < 0.15$ ,  $0.0015 < \xi < 0.5$  and  $0.1 < \xi < 0.5$ . We obtain 95% confidence level sensitivity limits on the unparticle couplings for various integrated luminosities.

---

\*inancsahin@karaelmas.edu.tr

†sceminan@cumhuriyet.edu.tr

## I. INTRODUCTION

The Large Hadron Collider (LHC) generates high energetic proton-proton collisions with a luminosity of  $\mathcal{L} = 10^{34} \text{cm}^{-2} \text{s}^{-1}$ . It provides high statistics data at high energies. On the other hand hadronic interactions generally involve serious backgrounds which have to be managed. Recently a new phenomenon called exclusive production was observed in the measurements of CDF collaboration [1, 2, 3, 4, 5, 6, 7] and its physics potential has being studied at the LHC [8, 9, 10, 11, 12, 13, 14, 15]. Complementary to proton-proton interactions, studies of exclusive production of leptons and heavy particles might be possible and opens new field of studying very high energy photon-photon and photon-proton interactions.

The exclusive production  $pp \rightarrow pXp$ , provides a clean environment due to absence of the proton remnants. ATLAS and CMS collaborations have a program of forward physics with extra detectors located in a region nearly 100m-400m from the interaction point. These forward detector equipment allows us to detect intact scattered protons after the collision. Therefore the processes which spoil the proton structure, can be easily discerned from the exclusive photo-production processes. By use of forward detector equipment we can eliminate many serious backgrounds. This is one of the advantages of the exclusive photo-production processes. Moreover photon-induced reactions are electromagnetic in nature and due to absence of the proton remnants it is free from almost all backgrounds. One possible background is the proton dissociation into baryon excitations. But this background can be eliminated effectively by imposing a cut on the transverse momentum of the photon or lepton pair [10]. It was argued in [10] that photon-induced lepton pair production is one of the most clean channels at the LHC when the acceptance cuts in place.

In this work we investigate the potential of exclusive  $pp \rightarrow p\ell^-\ell^+p$  and  $pp \rightarrow p\gamma\gamma p$  reactions at the LHC to probe unparticles. Unparticles are non-integral number  $d_U$  of particles. They are manifestations of a possible scale invariant sector of the new physics that may interact weakly with the standard model (SM) fields [16, 17, 18]. At low energies several effective interaction terms between unparticles and SM particles can be considered. In our calculations we consider the following effective interaction operators between SM fields and unparticles that satisfy the SM gauge symmetry [19]:

$$\frac{\lambda_S}{\Lambda_U^{d_U-1}} \bar{f} f \mathcal{O}_U, \quad \frac{\lambda_{PS}}{\Lambda_U^{d_U-1}} \bar{f} i \gamma^5 f \mathcal{O}_U, \quad \frac{\lambda_V}{\Lambda_U^{d_U}} \bar{f} \gamma^\mu f (\partial_\mu \mathcal{O}_U), \quad \frac{\kappa}{\Lambda_U^{d_U}} G_{\mu\nu} G^{\mu\nu} \mathcal{O}_U \quad (1)$$

$$- \frac{1}{4} \frac{\lambda_2}{\Lambda_U^{d_U}} \bar{\psi} i (\gamma_\mu D_\nu + \gamma_\nu D_\mu) \psi \mathcal{O}_U^{\mu\nu}, \quad \frac{\lambda'_2}{\Lambda_U^{d_U}} G_{\mu\alpha} G_\nu^\alpha \mathcal{O}_U^{\mu\nu} \quad (2)$$

where  $D_\mu = \partial_\mu + ig \frac{\tau^a}{2} W_\mu^a + ig' \frac{Y}{2} B_\mu$  is the covariant derivative,  $G^{\alpha\beta}$  denotes the gauge field strength.  $f$  stands for a SM fermion and  $\psi$  is the SM fermion doublet or singlet.  $\mathcal{O}_U$  and  $\mathcal{O}_U^{\mu\nu}$  represent the scalar and tensor unparticle fields. Feynman rules for these operators were given in [19].

Two-point functions for unparticles can be obtained by imposing scale invariance (or conformal invariance) [16, 17, 18, 20]. Requiring scale invariance, the Feynman propagators for the scalar and tensor unparticles are given respectively by

$$\Delta(P^2) = i \frac{A_{d_U}}{2 \sin(d_U \pi)} (-P^2)^{d_U-2} \quad (3)$$

$$\Delta(P^2)_{\mu\nu,\rho\sigma} = i \frac{A_{d_U}}{2 \sin(d_U \pi)} (-P^2)^{d_U-2} T_{\mu\nu,\rho\sigma}(P) \quad (4)$$

where,

$$A_{d_U} = \frac{16\pi^{\frac{5}{2}}}{(2\pi)^{2d_U}} \frac{\Gamma(d_U + \frac{1}{2})}{\Gamma(d_U - 1) \Gamma(2d_U)} \quad (5)$$

$$T_{\mu\nu,\rho\sigma}(P) = \frac{1}{2} \left[ \pi_{\mu\rho}(P) \pi_{\nu\sigma}(P) + \pi_{\mu\sigma}(P) \pi_{\nu\rho}(P) - \frac{2}{3} \pi_{\mu\nu}(P) \pi_{\rho\sigma}(P) \right] \quad (6)$$

$$\pi_{\mu\nu}(P) = -g_{\mu\nu} + \frac{P_\mu P_\nu}{P^2} \quad (7)$$

Conformal invariance can also be used to fix unparticle two-point functions. Conformal invariance leads to the same propagator for the scalar unparticles. But the tensor unparticle propagator is modified to a different form [20]. In Refs.[20, 21] theoretical bounds on the scale dimension were obtained from unitarity constraints. The scaling dimension for the scalar unparticle is constrained as  $d_U \geq 1$ . This constraint is valid in both conformal and scale

invariance. Scale invariance restricts the scaling dimension of tensor unparticle operator to  $d_U \geq 3$ . On the other hand, conformal invariant imposes a constraint of  $d_U \geq 4$ . We do not consider conformal invariance in the case of tensor unparticles since the lower bound of the scale dimension is large and therefore unparticle contribution is very suppressed. But we will present some results for the scale invariant tensor unparticles with the scale dimension  $d_U = 3.001$  and  $d_U = 3.01$ .

## II. EQUIVALENT PHOTON APPROXIMATION AND PHOTON-PHOTON FUSION

The photon-photon fusion can be described by equivalent photon approximation (EPA) [22]. In the exclusive production of an object X, two photons scattered from protons interact each other through the process  $pp \rightarrow p\gamma\gamma p \rightarrow pXp$ . In the framework of EPA, emitted photons have a low virtuality and scattered with small angles from the beam pipe. Therefore they are almost real and the cross section for the complete process  $pp \rightarrow p\gamma\gamma p \rightarrow pXp$  can be obtained by integrating the cross section for the subprocess  $\gamma\gamma \rightarrow X$  over the effective photon luminosity  $\frac{dL^{\gamma\gamma}}{dW}$

$$d\sigma = \int \frac{dL^{\gamma\gamma}}{dW} d\hat{\sigma}_{\gamma\gamma \rightarrow X}(W) dW \quad (8)$$

where W is the invariant mass of the two photon system and the effective photon luminosity is given by

$$\frac{dL^{\gamma\gamma}}{dW} = \int_{Q_{1,min}^2}^{Q_{max}^2} dQ_1^2 \int_{Q_{2,min}^2}^{Q_{max}^2} dQ_2^2 \int_{y_{min}}^{y_{max}} dy \frac{W}{2y} f_1\left(\frac{W^2}{4y}, Q_1^2\right) f_2(y, Q_2^2). \quad (9)$$

with

$$y_{min} = \text{MAX}(W^2/(4\xi_{max}E), \xi_{min}E), \quad y_{max} = \xi_{max}E. \quad (10)$$

$Q_{max}^2$  is taken to be  $2 \text{ GeV}^2$ ,  $y$  is the energy of one of the emitted photons from the proton,  $\xi_{min}$  and  $\xi_{max}$  are the acceptances of the forward detectors which tag protons with some momentum fraction loss  $\xi = (|\vec{p}| - |\vec{p}'|)/|\vec{p}|$ .  $f_1$  and  $f_2$  are the equivalent photon spectra. Equivalent photon spectrum of virtuality  $Q^2$  and energy  $E_\gamma$  is given by

$$f = \frac{dN}{dE_\gamma dQ^2} = \frac{\alpha}{\pi} \frac{1}{E_\gamma Q^2} \left[ \left(1 - \frac{E_\gamma}{E}\right) \left(1 - \frac{Q_{min}^2}{Q^2}\right) F_E + \frac{E_\gamma^2}{2E^2} F_M \right] \quad (11)$$

where

$$Q_{min}^2 = \frac{m_p^2 E_\gamma^2}{E(E - E_\gamma)}, \quad F_E = \frac{4m_p^2 G_E^2 + Q^2 G_M^2}{4m_p^2 + Q^2} \quad (12)$$

$$G_E^2 = \frac{G_M^2}{\mu_p^2} = \left(1 + \frac{Q^2}{Q_0^2}\right)^{-4}, \quad F_M = G_M^2, \quad Q_0^2 = 0.71 \text{ GeV}^2 \quad (13)$$

Here  $E$  is the energy of the proton beam which is related to the photon energy by  $E_\gamma = \xi E$  and  $m_p$  is the mass of the proton. The magnetic moment of the proton is taken to be  $\mu_p^2 = 7.78$ .  $F_E$  and  $F_M$  are functions of the electric and magnetic form factors.

The object  $X$  is detected by the central detectors while the intact scattered protons are detected by the forward detectors. ATLAS and CMS have central detectors with a pseudorapidity coverage  $|\eta| < 2.5$ . ATLAS Forward Physics (AFP) Collaboration proposed an acceptance of  $0.0015 < \xi < 0.15$  [14]. This acceptance allows to detect an object of mass in the interval  $100 \text{ GeV} < M < 800 \text{ GeV}$  with a good accuracy. There are also other scenarios with different acceptances of the forward detectors. CMS-TOTEM forward detector scenario spans  $0.0015 < \xi < 0.5$  and  $0.1 < \xi < 0.5$  [13, 23]. In Fig.1 in the left panel, we plot effective  $\gamma\gamma$  luminosity as a function of invariant mass of the two photon system for various forward detector acceptances.

In Ref.[10], exclusive lepton-pair production via photon photon fusion was proposed as a luminosity monitor for the LHC. It was discussed in detail in [10] that main possible background is the proton dissociation into baryon excitations;  $pp \rightarrow X + \ell^+ \ell^- + Y$  where  $X$  and  $Y$  are baryon excitations such as  $N^*$ ,  $\Delta$  isobars. It was shown in [10] that this background can be eliminated effectively by imposing a cut on the transverse momentum of the photon pair  $|\vec{q}_{1t} + \vec{q}_{2t}| < (10 - 30) \text{ MeV}$ . In actual experiment this cut can be placed on either photon pair or lepton pair. Similar arguments is also true for exclusive two photon production and same cut should be applied in order to eliminate the contamination from proton dissociation into baryon excitations. In all the results presented in this work we impose a cut of  $|\vec{q}_{1t} + \vec{q}_{2t}| < 30 \text{ MeV}$  on the transverse momentum of the photon pair. To see the effect of this cut on the effective  $\gamma\gamma$  luminosity, we plot  $dL^{\gamma\gamma}/dW$  as a function of invariant mass of the two photon system with and without a cut in the right panel of Fig.1.

### III. CROSS SECTIONS AND NUMERICAL ANALYSIS

#### A. Exclusive two lepton production

In the SM, the subprocess  $\gamma\gamma \rightarrow \ell^-\ell^+$  is described by t and u-channel tree-level diagrams. New physics contribution comes from s-channel unparticle exchange (Fig.2). The polarization summed amplitude square is given by the following formula

$$\begin{aligned}
|M|^2 = & 8g_e^4 tu \left( \frac{1}{t^2} + \frac{1}{u^2} \right) + \frac{4A_{d_U}^2 s^{(2d_U-4)}}{\sin^2(d_U\pi)} \frac{\kappa^2}{\Lambda_U^{(4d_U-2)}} (\lambda_{PS}^2 + \lambda_S^2) s^3 \\
& + \frac{A_{d_U}^2 s^{(2d_U-4)}}{2\sin^2(d_U\pi)} \left( \frac{\lambda_2^2 \lambda_2'^2}{\Lambda_U^{4d_U}} \right) ut(t^2 + u^2) \\
& - 4g_e^2 A_{d_U} s^{(d_U-2)} \left( \frac{\lambda_2 \lambda_2'}{\Lambda_U^{2d_U}} \right) \cot(d_U\pi) (t^2 + u^2)
\end{aligned} \tag{14}$$

where  $g_e = \sqrt{4\pi\alpha}$ , s, t and u are the Mandelstam variables and we omit the mass of leptons. We see from this amplitude that scalar unparticle contribution does not interfere with the SM. Therefore scalar unparticle contribution is always additive. On the other hand, tensor contribution interfere with the SM. The trigonometric functions  $\cos(d_U\pi)$  in the interference terms originate from the complex phase associated with the s-channel propagator and may lead to interesting interference effects with the standard model amplitudes. We also see from (14) that contribution of the coupling  $\lambda_{PS}$  to the cross section is equal to the contribution of the coupling  $\lambda_S$ . It is then impossible to distinguish  $\lambda_{PS}$  from  $\lambda_S$  and therefore we only consider the coupling  $\lambda_S$  in our numerical calculations. The scalar unparticle coupling  $\lambda_V$  does not contribute to the process since the unparticle couples to the on-mass-shell current  $\ell^-\ell^+$ .

We consider three different forward detector acceptances;  $0.0015 < \xi < 0.15$ ,  $0.0015 < \xi < 0.5$  and  $0.1 < \xi < 0.5$ . In Fig.3 we plot cross section of  $pp \rightarrow p\ell^-\ell^+p$  as a function of the transverse momentum cut on the final leptons. We observe from the figure that cross sections including unparticle contributions deviate from the SM as the  $p_t$  cut increases. Unparticle contributions and the SM are well separated from each other for large values of the  $p_t$  cut. Furthermore, we observe from (14) that the SM contribution is highly peaked in the forward and backward directions due to  $t, u = 0$  poles whereas the unparticle contribution is rather flat. Therefore both angular distribution or the  $p_t$  cut can be used to improve sensitivity

bounds.

During statistical analysis we use two different approach. In the first approach we impose cuts on the transverse momentum of the final leptons to suppress the SM cross section. We make the number of SM event less than 0.5. Then it is very appropriate to set bounds on the couplings using a Poisson distribution. We set a cut of  $p_t > 420$  GeV for  $0.0015 < \xi < 0.15$  and a cut of  $p_t > 460$  GeV for  $0.0015 < \xi < 0.5$  on the final leptons to improve the bounds. These values for the  $p_t$  cut make the SM event less than 0.5 for a luminosity of  $200 \text{ fb}^{-1}$ . In the case  $0.1 < \xi < 0.5$ , invariant mass of the final leptons is greater than 1400 GeV due to the high lower bound of  $\xi$ . The SM cross section is very small and therefore it does not need to impose a high  $p_t$  cut. We consider a cut of  $p_t > 30\text{GeV}$  for  $0.1 < \xi < 0.5$ .

In the second approach we have obtained sensitivity bounds using the simple  $\chi^2$  criterion from angular distribution

$$\chi^2 = \sum_{i=\text{bins}} \left( \frac{\sigma_{SM}^i - \sigma_{NEW}^i}{\sigma_{SM}^i \Delta_{exp}^i} \right)^2 \quad (15)$$

where

$$\sigma_{SM}^i = \int_{z_i}^{z_{i+1}} \frac{d\sigma_{SM}}{dz} dz \quad (16)$$

$$\sigma_{NEW}^i = \int_{z_i}^{z_{i+1}} \frac{d\sigma_{NEW}}{dz} dz \quad (17)$$

$$\Delta_{exp}^i = \sqrt{\delta_{stat.}^i{}^2 + \delta_{syst.}^i{}^2}, \quad z = \cos \theta \quad (18)$$

Here, subscript "NEW" represents the cross section including unparticle contributions.  $\delta_{stat.}$  and  $\delta_{syst.}$  are the statistical and systematic errors. We have divided the range of  $\cos \theta$  into six equal pieces for the binning procedure and have considered at least 100 events in each bin. We impose only a pseudo-rapidity cut of  $|\eta| < 2.5$  which is necessary for the central detector acceptance.

For a concrete result we have obtained 95% confidence level (C.L.) limits on the unparticle couplings. The number of observed events is assumed to be equal to the SM prediction  $N_{obs} = 0.9 L \sigma_{SM}$  where  $L$  is the integrated luminosity and 0.9 is the QED two-photon survival probability [24]. We assume that electrons and muons in the final state can be observed in the central detectors with an acceptance cut of  $|\eta| < 2.5$ . In Fig.4-6 we present the sensitivity of  $pp \rightarrow p\ell^-\ell^+p$  to the product of scalar unparticle couplings  $\kappa\lambda_S$  from a

Poisson distribution. Sensitivity limits are given as a function of integrated LHC luminosity for the acceptances of  $0.0015 < \xi < 0.5$ ,  $0.0015 < \xi < 0.15$  and  $0.1 < \xi < 0.5$ . Since the scalar unparticle contribution is symmetric in the negative and positive intervals of the coupling we present our results only for positive  $\kappa\lambda_S$ . We see from the figures that the decrease in  $d_U$  generally improves the sensitivity limits. The most sensitive results are obtained at  $d_U = 1.01$ . On the other hand, limits for  $d_U = 1.9$  are sensitive than the limits for  $d_U = 1.8$ . This is reasonable from  $\sin^2(d_U\pi)$  dependence of the denominator of the scalar unparticle contribution (14). Limits on the tensor unparticle couplings are given in Fig.7 and Fig.8 from a Poisson distribution for the acceptances  $0.0015 < \xi < 0.5$  and  $0.1 < \xi < 0.5$  respectively. Limits for  $0.0015 < \xi < 0.15$  are too weak compared with other cases so we do not plot them. We see from the figures that limits for  $0.0015 < \xi < 0.5$  and  $0.1 < \xi < 0.5$  cases are almost the same. This originates from the fact that at low energies tensor unparticle contribution is very suppressed and the main contribution comes from high energy region.

In Fig.4-6,  $p_t$  cuts on the final leptons are proposed considering a luminosity of  $200 \text{ fb}^{-1}$ . On the other hand, these cuts are not the optimum ones for other luminosity values. For a given luminosity, limits on the unparticle couplings can be improved by adjusting the  $p_t$  cut on the final leptons. To this purpose, we present Table I and Table II where we take into account different  $p_t$  cuts for different luminosities. We show that especially for small luminosity values, considerable improvement is obtained in the limits by adjusting the  $p_t$  cut. In Table III and Table IV we show 95%C.L. lower bounds on the energy scale  $\Lambda_U$  with the same luminosity values and  $p_t$  cuts of Tables I-II. In the tables the couplings are taken to be  $\kappa=\lambda_S=1$  and  $\lambda_{PS} = \lambda_2 = \lambda'_2 = 0$ .

In Fig.9 and Fig.10, we estimate 95% C.L. limits for scalar and tensor unparticle couplings using a simple  $\chi^2$  test without a systematic error. We do not estimate the limits for  $0.1 < \xi < 0.5$  case since the SM cross section is about  $1.1 \times 10^{-6} \text{ pb}$ . Therefore number of SM event is smaller than 1 even for a luminosity of  $200 \text{ fb}^{-1}$ . We see from Fig.9 and Fig.10 that limits rapidly get worse as the  $d_U$  increases. This behavior is common in the analysis from a Poisson distribution but deterioration rate is high in the  $\chi^2$  case. For example, when the detector acceptance is  $0.0015 < \xi < 0.5$ , limits on the scalar unparticle couplings from Poisson distribution deteriorated by a factor of 7 as the  $d_U$  increases from 1.01 to 1.4. But this factor is approximately 40 in the  $\chi^2$  analysis. Therefore,  $\chi^2$  analysis from angular



distribution is favorable for small values of the scale dimension close to unity. Hence we do not give the limits on the scalar unparticle couplings for  $d_U > 1.5$ . But for comparison, we also give the limits on the tensor unparticle couplings for  $d_U = 3.001$  and  $3.01$  (Fig.10).

## B. Exclusive two photon production

The subprocess  $\gamma\gamma \rightarrow \gamma\gamma$  is absent in the SM at the tree-level. Scalar and tensor unparticles contribute to the process through t, u and s-channel diagrams (Fig.11). The polarization summed scattering amplitude for Fig.11 is given by [25]

$$\begin{aligned}
|M|^2 = & \frac{A_{d_U}^2}{\sin^2(d_U\pi)} \left\{ \frac{16\kappa^4}{\Lambda_U^{4d_U}} [|t|^{2d_U} + s^{2d_U} + |u|^{2d_U} + |t|^{d_U}|u|^{d_U} \right. \\
& + \cos(d_U\pi) (|t|^{d_U}s^{d_U} + s^{d_U}|u|^{d_U})] + \frac{\lambda_2'^4}{2\Lambda_U^{4d_U}} [s^{2d_U-4}(t^4 + u^4) \\
& + |t|^{2d_U-4}(s^4 + u^4) + |u|^{2d_U-4}(s^4 + t^4) + 2|t|^{d_U-2}|u|^{d_U-2}s^4 \\
& \left. + 2\cos(d_U\pi)s^{d_U-2}(|t|^{d_U-2}u^4 + |u|^{d_U-2}t^4) \right] \Big\} \quad (19)
\end{aligned}$$

When we compare this amplitude with the amplitude of  $\gamma\gamma \rightarrow \ell^-\ell^+$ , we see that unlike from amplitude (14), t and u-channel scalar unparticle exchange interfere with the s-channel one. The prominent advantage of the subprocess  $\gamma\gamma \rightarrow \gamma\gamma$  is that it isolates the couplings  $\kappa$  and  $\lambda_2'$ . As we have seen, this is not the case in  $\gamma\gamma \rightarrow \ell^-\ell^+$ .

SM background is originated from loop diagrams involving contributions from charged fermions and W bosons. In Fig.12 we plot SM expectation at 1-loop level using the form factors from Refs.[26, 27, 28]. We observe from the left panel of Fig.12 that the SM cross section rapidly grows when the energy decreases from approximately 200 GeV. This behavior originates from fermion loop contributions. We impose a cut of  $\sqrt{s_{\gamma\gamma}} > 250$  GeV on the invariant mass of final photons to reduce the contribution coming from fermion loops. (This constraint is automatically satisfied in  $0.1 < \xi < 0.5$  since  $E_{min} = 1400$  GeV.) Furthermore we impose a pseudo-rapidity cut of  $|\eta| < 0.88$  for the cases;  $0.0015 < \xi < 0.5$  and  $0.0015 < \xi < 0.15$ . These cuts effectively suppress SM loop contributions coming from fermion and W loops but do not spoil unparticle limits more than a factor of 1.5. This is reasonable since the main unparticle contribution comes from high energy region and it does not peak in the forward and backward directions. On the other hand, we see from the right panel of Fig.12

that SM cross section peaks in the forward and backward directions. Total SM cross sections from W and fermion loops are;  $3.50 \times 10^{-7} \text{pb}$  for  $0.0015 < \xi < 0.15$  and  $3.52 \times 10^{-7} \text{pb}$  for  $0.0015 < \xi < 0.5$  when the mentioned cuts in place. Therefore they are negligible even with a luminosity of  $200 \text{fb}^{-1}$ . In  $0.1 < \xi < 0.5$  case with  $|\eta| < 2.5$  loop contributions are much more smaller. Total SM cross section is  $2.60 \times 10^{-8} \text{pb}$ .

In order to obtain more realistic results, we take into account a photon efficiency of 90% for each final photons in the numerical calculations [29, 30]. In Fig.13-15 we plot sensitivity of  $pp \rightarrow p\gamma\gamma p$  to scalar unparticle coupling  $\kappa$  as a function of integrated LHC luminosity for the acceptances of  $0.0015 < \xi < 0.5$ ,  $0.0015 < \xi < 0.15$  and  $0.1 < \xi < 0.5$ . The most sensitive results are obtained in  $0.0015 < \xi < 0.5$  for  $d_U = 1.01$  and  $1.1$ . But  $0.1 < \xi < 0.5$  case gives better limits for  $d_U > 1.1$ . In Fig.16 we present the limits on tensor unparticle coupling  $\lambda'_2$  for the scale dimensions  $d_U = 3.001$  and  $d_U = 3.01$ . We observe from the figure that the limits for  $0.0015 < \xi < 0.5$  and  $0.1 < \xi < 0.5$  cases are close to each other. Therefore forward detectors with acceptances  $0.0015 < \xi < 0.5$  and  $0.1 < \xi < 0.5$  have almost same potential to probe tensor unparticle contribution through the process  $pp \rightarrow p\gamma\gamma p$ .

Lower bounds on the energy scale  $\Lambda_U$  are obtained as a function of integrated LHC luminosity in Fig.17. A comparison with Table.III shows that  $pp \rightarrow p\ell^-\ell^+p$  is more sensitive to  $\Lambda_U$  for the values of the scale dimension which are close to unity such as  $d_U = 1.01$  and  $d_U = 1.1$ . On the other hand, the process  $pp \rightarrow p\gamma\gamma p$  is more sensitive to the energy scale for the values of the scale dimension between  $1.4 - 1.9$ .

#### IV. CONCLUSIONS

Current experimental restrictions on unparticle couplings were widely studied in the literature. Although there still remains some reactions which was not examined, task to find current experimental limits is almost completed. LHC has started operating and its potential to probe unparticles has been under research [31, 32, 33, 34, 35, 36, 37, 38, 39, 40, 41, 42]. Limits from LHC have been provided by two photon production via  $gg, q\bar{q} \rightarrow \gamma\gamma$  [38]. A comparison of our limits with the limits of  $gg, q\bar{q} \rightarrow \gamma\gamma$  is not possible in general since the reactions involve different type of couplings. If we assume that unparticle couplings to quarks and gluons are equal to its couplings to leptons and photons then we conclude that our limits are weaker than the limits obtained through these reactions at the LHC but

stronger than the limits obtained at the Tevatron [38]. On the other hand, exclusive  $\ell^-\ell^+$  and  $\gamma\gamma$  production through  $\gamma\gamma$  fusion provide very clean environment due to absence of the proton remnants. Therefore any signal which conflicts with the SM predictions would be a convincing evidence for new physics.

The exclusive two photon production  $pp \rightarrow p\gamma\gamma p$  isolates the couplings  $\gamma\gamma U$ ,  $\gamma\gamma U^{\mu\nu}$ . This is a prominent advantage of  $pp \rightarrow p\gamma\gamma p$  and it can not be achieved in any other process at the LHC. In the future,  $\gamma\gamma$  colliders are expected to be designed complementary to linear  $e^+e^-$  colliders [43]. At the  $\gamma\gamma$  mode of a linear collider,  $\gamma\gamma U$  and  $\gamma\gamma U^{\mu\nu}$  couplings can be probed with a high precision [25, 44, 45].

The process  $pp \rightarrow p\ell^-\ell^+p$  was proposed as a luminosity monitor for the LHC [10]. If it is used to measure luminosity then it is important to know its sensitivity to new physics for a given acceptance range. We have explored sensitivity of  $pp \rightarrow p\ell^-\ell^+p$  to unparticles with three different forward detector acceptances. We show that  $0.1 < \xi < 0.5$  case is least sensitive to scalar unparticles for  $d_U = 1.01 - 1.2$  but  $0.0015 < \xi < 0.15$  case is least sensitive for  $d_U = 1.3 - 1.9$ . Tensor unparticle contribution rapidly grows with energy. Forward detector acceptance of  $0.0015 < \xi < 0.15$  is least sensitive to tensor unparticle contribution.

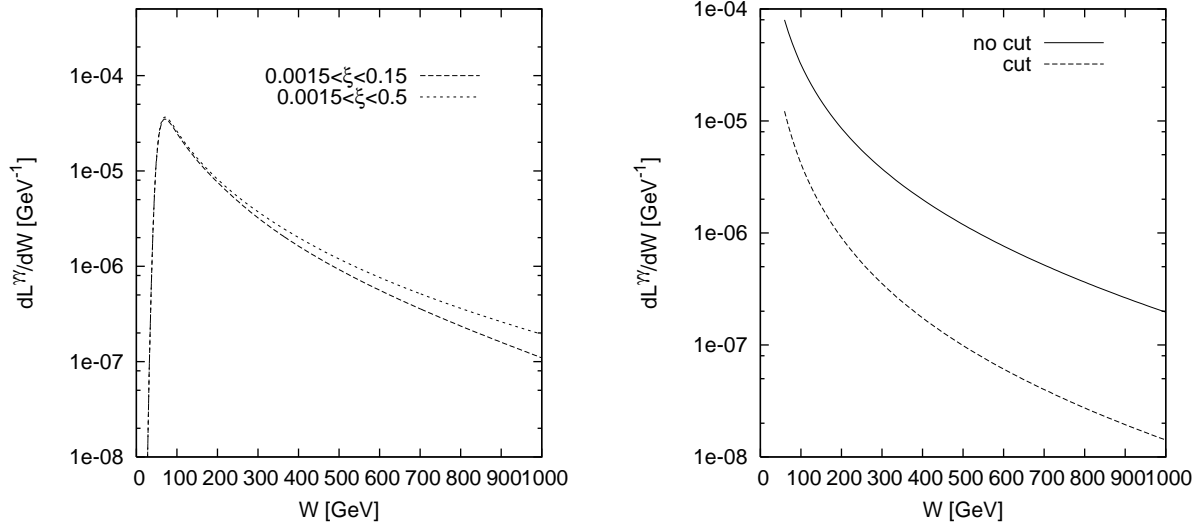


FIG. 1: Effective  $\gamma\gamma$  luminosity as a function of the invariant mass of the two photon system. Figure on the left shows effective luminosity for forward detector acceptances  $0.0015 < \xi < 0.15$  and  $0.0015 < \xi < 0.5$ . Figure on the right represents the cases with and without a cut on transverse momentum of the photon pair  $|\vec{q}_{1t} + \vec{q}_{2t}| < 30\text{MeV}$ . In the right panel, we do not consider any acceptance i.e.,  $\xi$  is taken to be in the interval  $0 < \xi < 1 - m_p/E$  where  $m_p$  is the mass and  $E$  is the energy of the incoming proton.

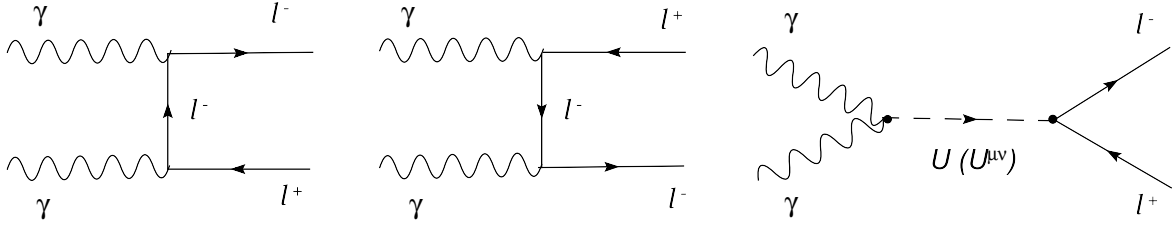


FIG. 2: Tree-level Feynman diagrams for the subprocess  $\gamma\gamma \rightarrow \ell^-\ell^+$ .

- 
- [1] A. Abulencia *et al.* (CDF Collaboration), Phys. Rev. Lett. **98**, 112001 (2007).
  - [2] T. Aaltonen *et al.* (CDF Collaboration), Phys. Rev. Lett. **99**, 242002 (2007).
  - [3] T. Aaltonen *et al.* (CDF Run II Collaboration), Phys. Rev. D **77**, 052004 (2008).
  - [4] T. Aaltonen *et al.* (CDF Collaboration), Phys. Rev. Lett. **102**, 242001 (2009).

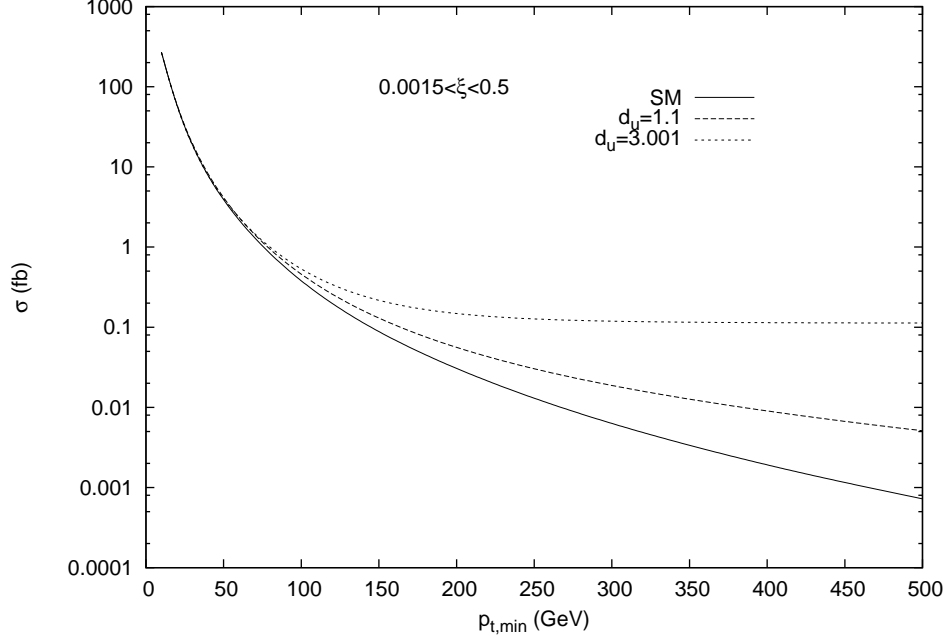


FIG. 3: Cross section of  $pp \rightarrow p\ell^-\ell^+p$  as a function of the transverse momentum cut on the final leptons. Solid line is for the SM and dotted lines  $d_u = 1.1$  and  $d_u = 3.001$  include scalar and tensor unparticle contributions respectively. Scalar unparticle couplings are taken to be  $\kappa = \lambda_S = 1$  and tensor unparticle couplings are taken to be  $\lambda'_2 = 1$  and  $\lambda_2 = 10^3$ .

- [5] T. Aaltonen *et al.* (CDF Collaboration), Phys. Rev. Lett. **102**, 222002 (2009).
- [6] O. Kepka and C. Royon, Phys. Rev. D **76**, 034012 (2007).
- [7] M. Rangel, C. Royon, G. Alves, J. Barreto, and R. Peschanski, Nucl. Phys. B **774**, 53 (2007).
- [8] S. M. Lietti, A. A. Natale, C. G. Roldao and R. Rosenfeld, Phys. Lett. B **497**, 243 (2001).
- [9] K. Piotrkowski, Phys. Rev. D **63**, 071502(R) (2001).
- [10] V. A. Khoze, A. D. Martin, R. Orava and M. G. Ryskin, Eur. Phys. J. C **19**, 313 (2001).
- [11] V. P. Goncalves and M. V. T. Machado, Phys. Rev. D **75**, 031502(R) (2007).
- [12] M. V. T. Machado, Phys. Rev. D **78**, 034016 (2008).
- [13] O. Kepka and C. Royon Phys. Rev. D **78**, 073005 (2008).
- [14] M.G. Albrow *et al.* (FP420 R and D Collaboration), arXiv:0806.0302.
- [15] S. Atağ, S. C. İnan and İ. Şahin, arXiv:0904.2687 [hep-ph].
- [16] H. Georgi, Phys. Rev. Lett. **98**, 221601 (2007).
- [17] H. Georgi, Phys. Lett. B **650**, 275 (2007).

- [18] K. Cheung, W.-Y. Keung and T.-C. Yuan, Phys. Rev. Lett. **99**, 051803 (2007).
- [19] K. Cheung, W.-Y. Keung and T.-C. Yuan, Phys. Rev. D **76**, 055003 (2007).
- [20] B. Grinstein, K. Intriligator, I. Z. Rothstein, Phys. Lett. B **662**, 367374 (2008).
- [21] Yu Nakayama, Phys. Rev. D **76**, 105009 (2007).
- [22] V. M. Budnev, I. F. Ginzburg, G. V. Meledin and V. G. Serbo, Phys. Rep. **15**, 181 (1975).
- [23] V. Avati and K. Osterberg, Report No. CERN-TOTEM-NOTE-2005-002, 2006.
- [24] V. A. Khoze, A. D. Martin and M. G. Ryskin, Eur. Phys. J. C **23**, 311 (2002).
- [25] C.-F. Chang, K. Cheung and T.-C. Yuan, Phys. Lett. B **664**, 291, (2008).
- [26] G. Jikia and A. Tkabladze, Phys. Lett. B, **323**, 453 (1994).
- [27] G. J. Gounaris, P. I. Porfyriadis and F. M. Renard, Phys. Lett. B, **452**, 76 (1999).
- [28] G. J. Gounaris, P. I. Porfyriadis and F. M. Renard, Eur. Phys. J. C, **9**, 673 (1999).
- [29] J. Colas *et al.*, Nucl. Instr. and Meth. in Phys. Res. A **550**, 96 (2005).
- [30] M.D. Baker, ATL-PHYS-PROC-2009-059.
- [31] P. Mathews, V. Ravindran, Phys. Lett. B, **657**, 198 (2007).
- [32] R. Mohanta, A. K. Giri, Phys. Rev. D **76**, 075015 (2007).
- [33] T. G. Rizzo, JHEP 0710:044,(2007).
- [34] T. G. Rizzo, Phys. Lett. B **665**, 361 (2008).
- [35] T. G. Rizzo, JHEP 0811:039,(2008).
- [36] A. T. Alan, N. K. Pak, Europhys. Lett. **84**, 11001 (2008).
- [37] M. C. Kumar, P. Mathews, V. Ravindran and A. Tripathi, Phys. Rev. D **77**, 055013 (2008).
- [38] J. L. Feng, A. Rajaraman and H. Tu, Phys. Rev. D **77**, 075007 (2008).
- [39] D. Choudhury, D. K. Ghosh, Int. J. Mod. Phys. A **23**, 2579 (2008).
- [40] M. C. Kumar, P. Mathews, V. Ravindran and A. Tripathi, Phys. Rev. D **79**, 075012 (2009).
- [41] N. Agarwal, M. C. Kumar, P. Mathews, V. Ravindran, A. Tripathi, arXiv:0903.0202 [hep-ph].
- [42] M. Arai, N. Okada and K. Smolek, Phys. Rev. D **79**, 074019 (2009).
- [43] J. A. Aguilar-Saavedra *et al.*, TESLA Technical Design Report Part III, DESY-2001-011.
- [44] T. Kikuchi, N. Okada, M. Takeuchi, Phys. Rev. D **77**, 094012 (2008).
- [45] O. Cakir, K. O. Ozansoy, Eur. Phys. J. C **56**, 279 (2008).

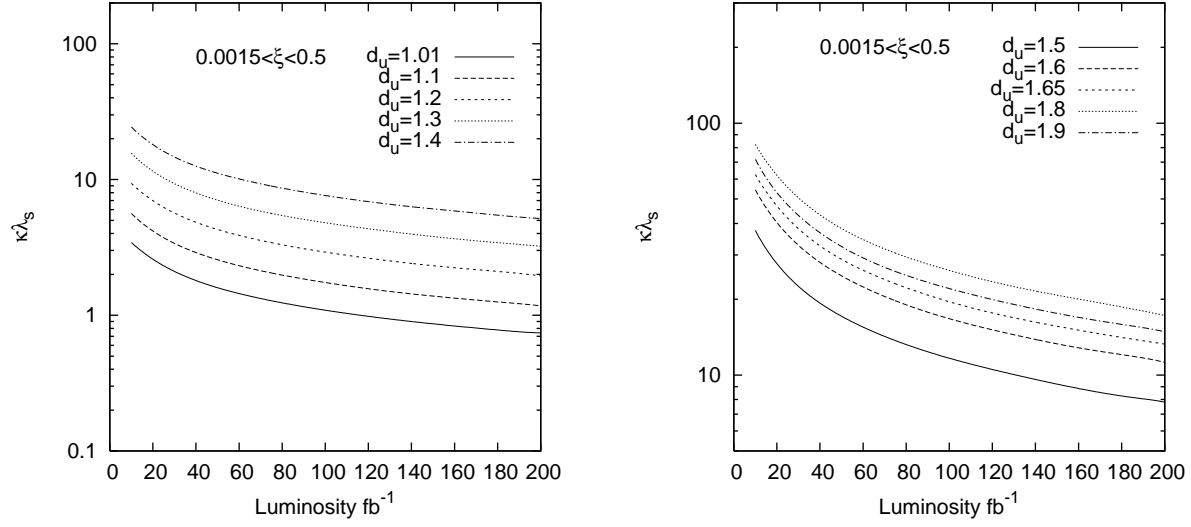


FIG. 4: 95% C.L sensitivity of  $pp \rightarrow p\ell^-\ell^+p$  to the product of scalar unparticle couplings  $\kappa\lambda_S$  as a function of integrated LHC luminosity for an acceptance of  $0.0015 < \xi < 0.5$ . Various values of the scale dimension are stated on the figures. We impose the cuts;  $|\vec{q}_{1t} + \vec{q}_{2t}| < 30\text{MeV}$ ,  $|\eta| < 2.5$  and  $p_t > 460\text{GeV}$ .  $\Lambda_U$  is taken to be 3 TeV.

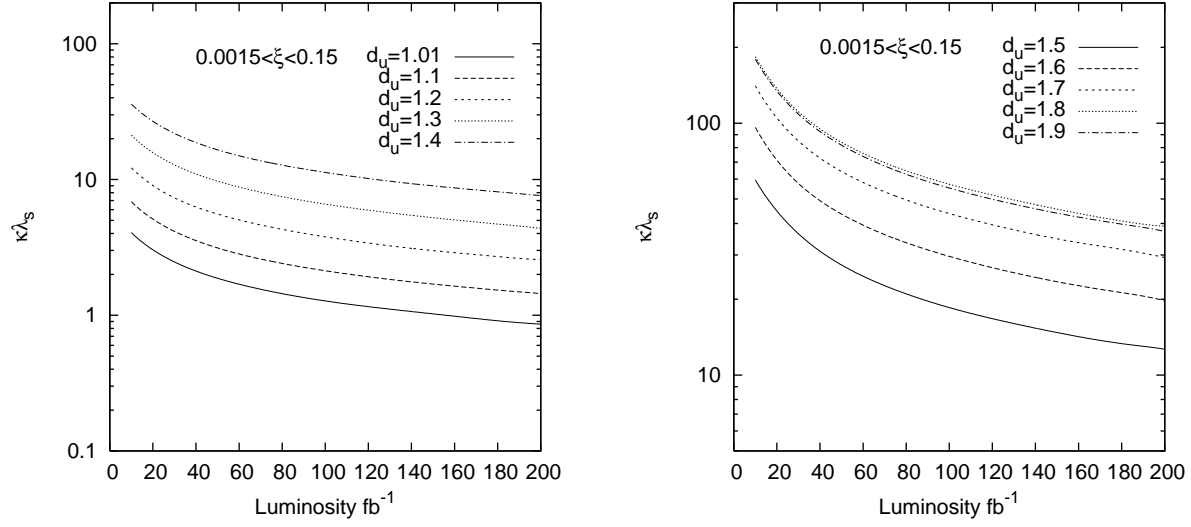


FIG. 5: 95% C.L sensitivity of  $pp \rightarrow p \ell^- \ell^+ p$  to the product of scalar unparticle couplings  $\kappa \lambda_S$  as a function of integrated LHC luminosity for an acceptance of  $0.0015 < \xi < 0.15$ . Various values of the scale dimension are stated on the figures. We impose the cuts;  $|\vec{q}_{1t} + \vec{q}_{2t}| < 30\text{MeV}$ ,  $|\eta| < 2.5$  and  $p_t > 420\text{GeV}$ .  $\Lambda_U$  is taken to be 3 TeV.



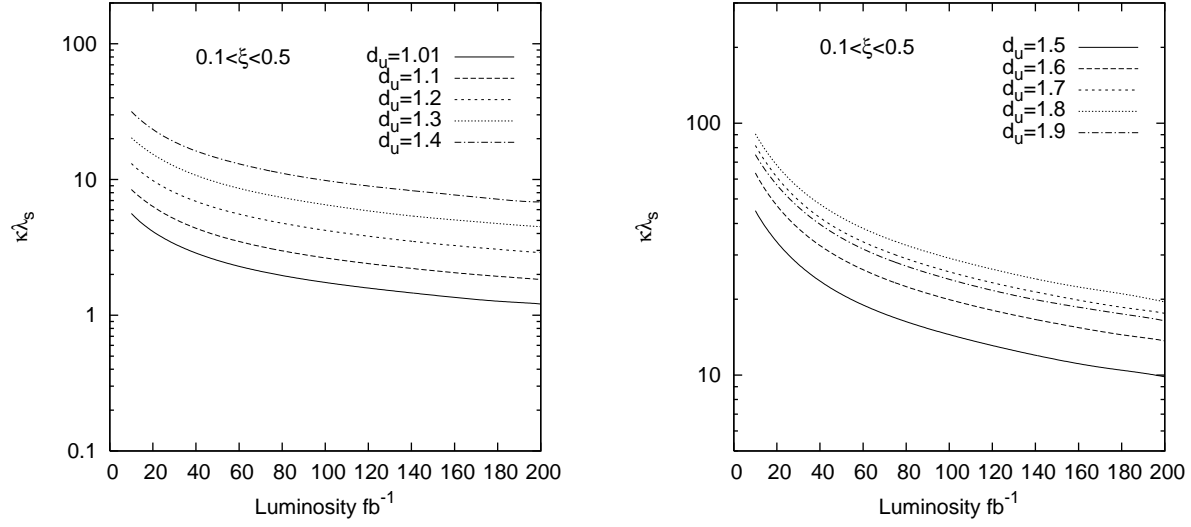


FIG. 6: 95% C.L sensitivity of  $pp \rightarrow p\ell^-\ell^+p$  to the product of scalar unparticle couplings  $\kappa\lambda_S$  as a function of integrated LHC luminosity for an acceptance of  $0.1 < \xi < 0.5$ . Various values of the scale dimension are stated on the figures. We impose the cuts;  $|\vec{q}_{1t} + \vec{q}_{2t}| < 30\text{MeV}$ ,  $|\eta| < 2.5$  and  $p_t > 30\text{GeV}$ .  $\Lambda_U$  is taken to be 3 TeV.

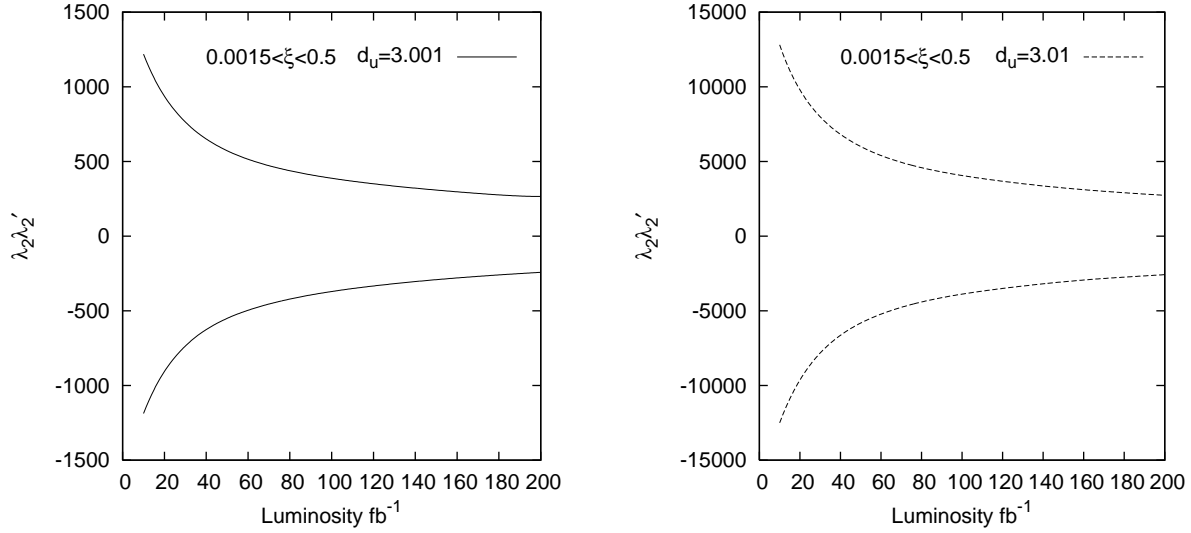


FIG. 7: The same as Fig.4 but for product of tensor unparticle couplings  $\lambda_2\lambda'_2$ .

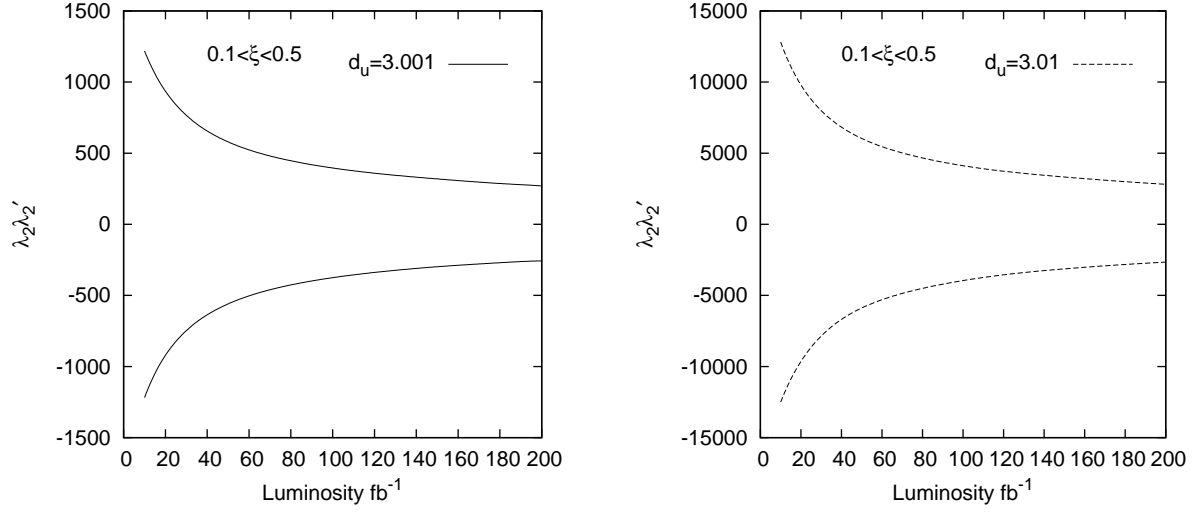


FIG. 8: The same as Fig.6 but for product of tensor unparticle couplings  $\lambda_2\lambda'_2$ .

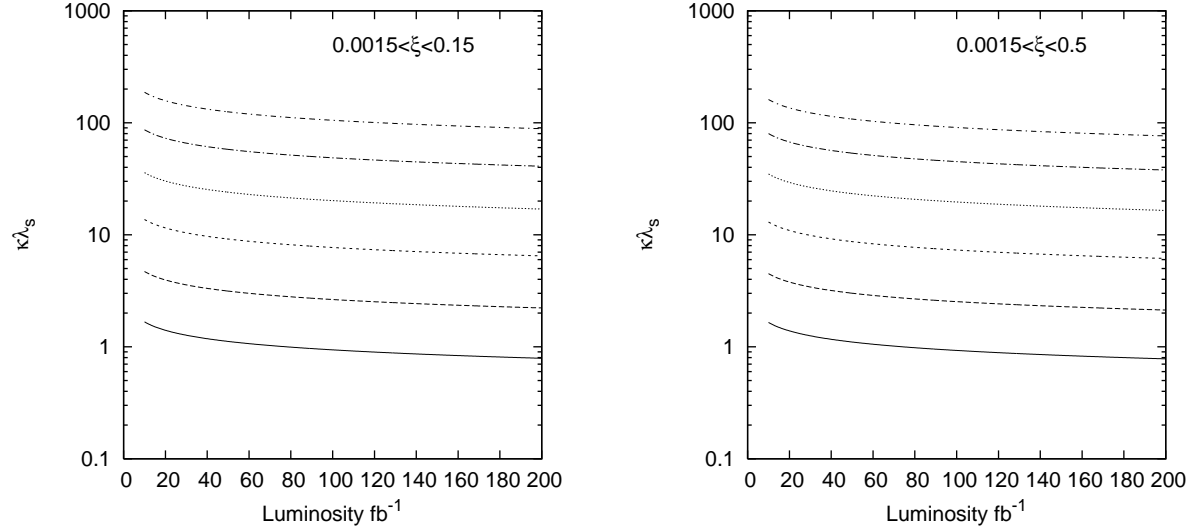


FIG. 9: 95% C.L sensitivity of  $pp \rightarrow p\ell^-\ell^+p$  to the product of scalar unparticle couplings  $\kappa\lambda_S$  as a function of integrated LHC luminosity for the acceptances  $0.0015 < \xi < 0.15$  (left panel) and  $0.0015 < \xi < 0.5$  (right panel). Limits are estimated using a simple  $\chi^2$  test from angular distribution without a systematic error. Curves from bottom to top correspond to increasing values of  $d_U = 1.01, 1.1, 1.2, 1.3, 1.4$  and  $1.5$ . We impose the cuts;  $|\vec{q}_{1t} + \vec{q}_{2t}| < 30\text{MeV}$ ,  $|\eta| < 2.5$  and  $\Lambda_U$  is taken to be 3 TeV.

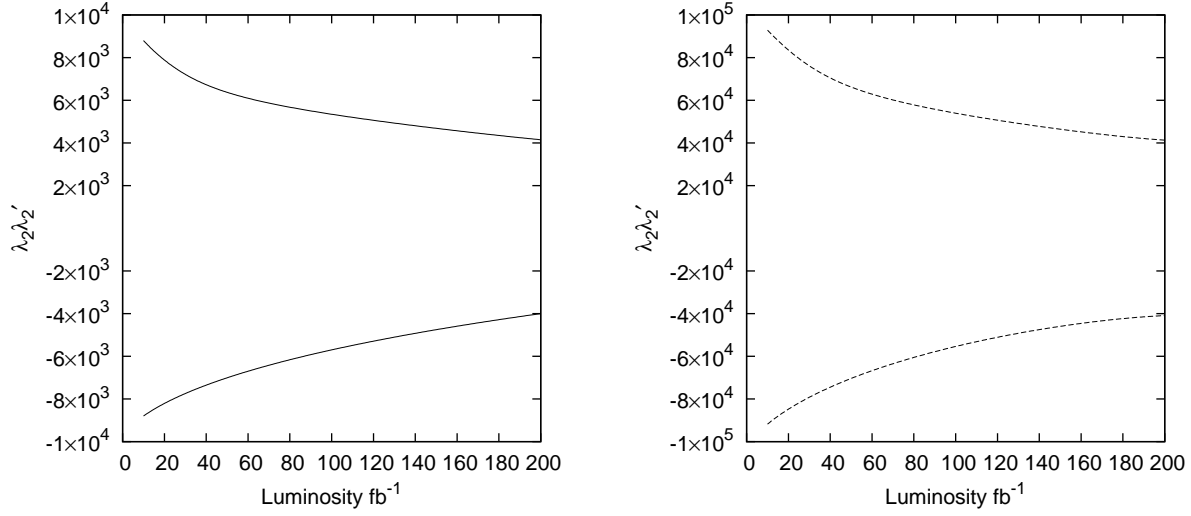


FIG. 10: 95% C.L sensitivity of  $pp \rightarrow p\ell^-\ell^+p$  to the product of tensor unparticle couplings  $\lambda_2\lambda_2'$  as a function of integrated LHC luminosity for the acceptance  $0.0015 < \xi < 0.5$ . Limits are estimated using a simple  $\chi^2$  test from angular distribution without a systematic error. Solid line corresponds to the limit for  $d_U = 3.001$  (left panel) and the dotted line corresponds to  $d_U = 3.01$  (right panel). We impose the cuts;  $|\vec{q}_{1t} + \vec{q}_{2t}| < 30\text{MeV}$ ,  $|\eta| < 2.5$  and  $\Lambda_U$  is taken to be 3 TeV.

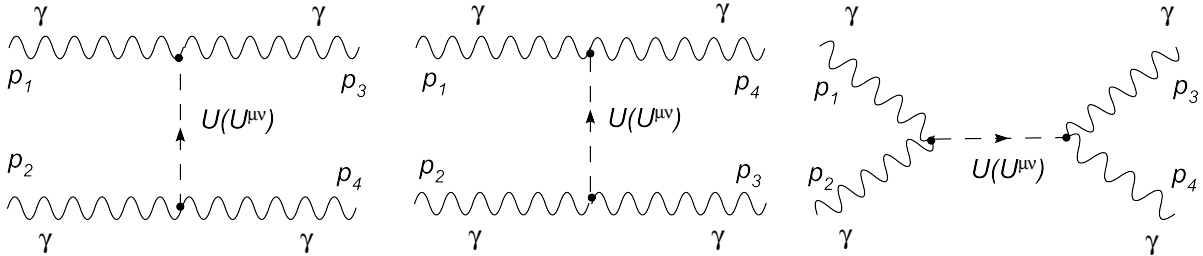


FIG. 11: Tree-level Feynman diagrams for the subprocess  $\gamma\gamma \rightarrow \gamma\gamma$ .

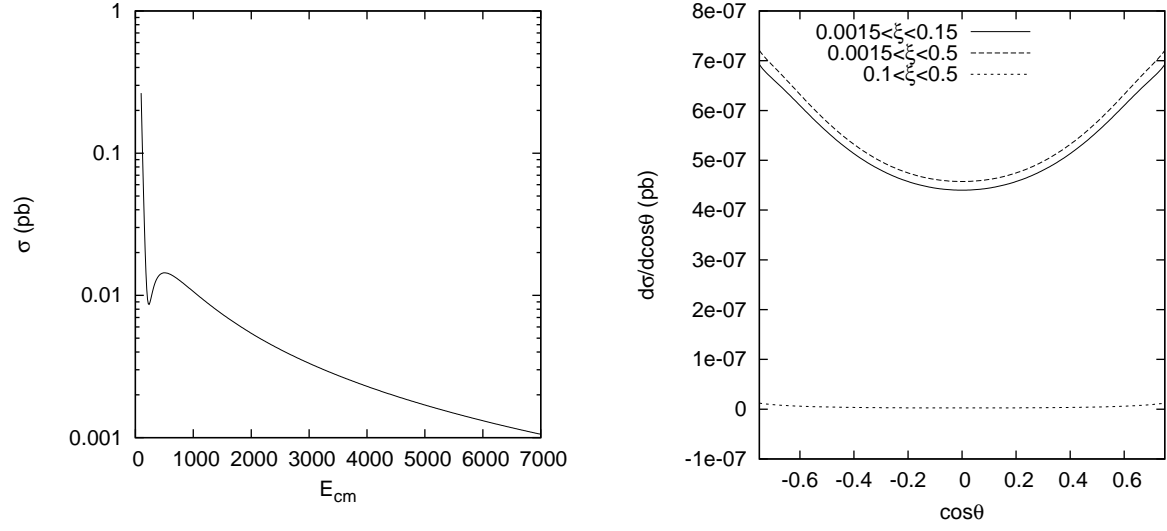


FIG. 12: Figure on the left shows total SM 1-loop contribution as a function of center of mass energy of the two photon system. Figure on the right shows angular distribution of the total SM 1-loop contributions for various forward detector acceptances stated on the figure. We impose a cut of  $|\cos\theta| < 0.86$  in the left panel.

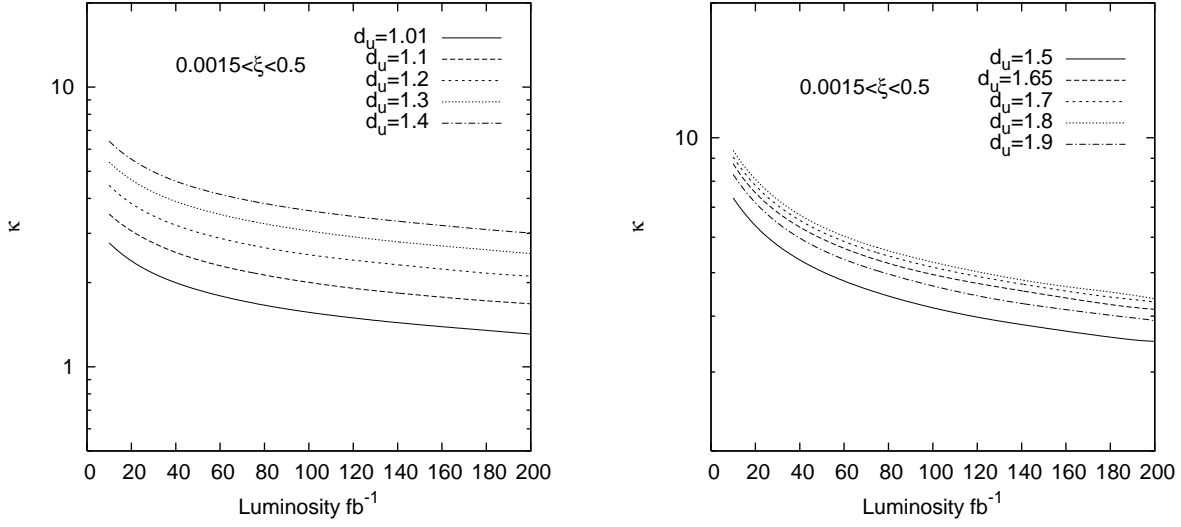


FIG. 13: 95% C.L sensitivity of  $pp \rightarrow p\gamma\gamma p$  to scalar unparticle coupling  $\kappa$  as a function of integrated LHC luminosity for an acceptance of  $0.0015 < \xi < 0.5$ . Various values of the scale dimension are stated on the figures. We impose the cuts;  $|\vec{q}_{1t} + \vec{q}_{2t}| < 30\text{MeV}$ ,  $\sqrt{s_{\gamma\gamma}} > 250\text{ GeV}$  and  $|\eta| < 0.88$ .  $\Lambda_U$  is taken to be 3 TeV.

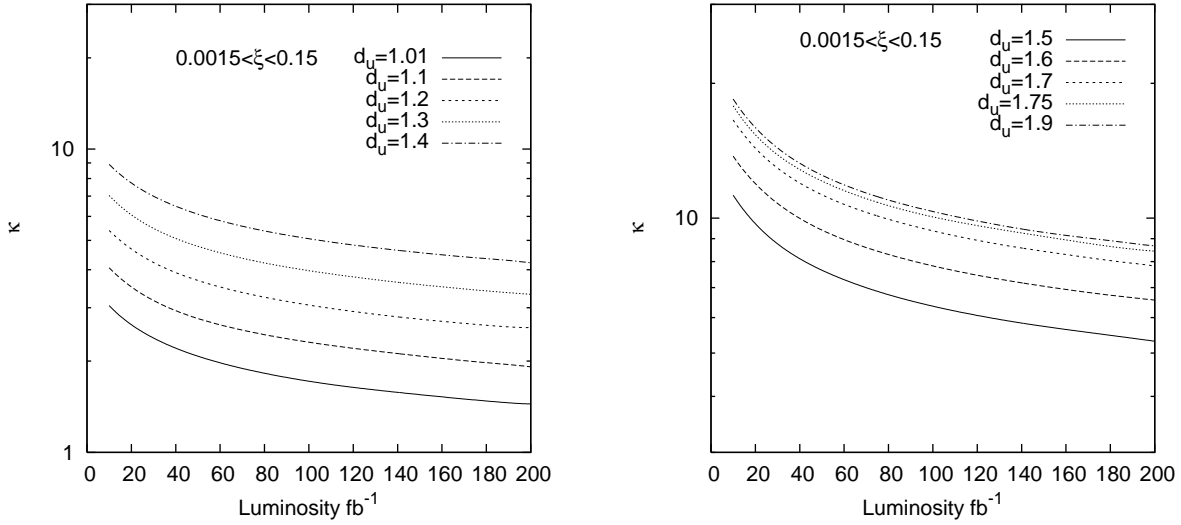


FIG. 14: The same as Fig.13 but for forward detector acceptance  $0.0015 < \xi < 0.15$ .

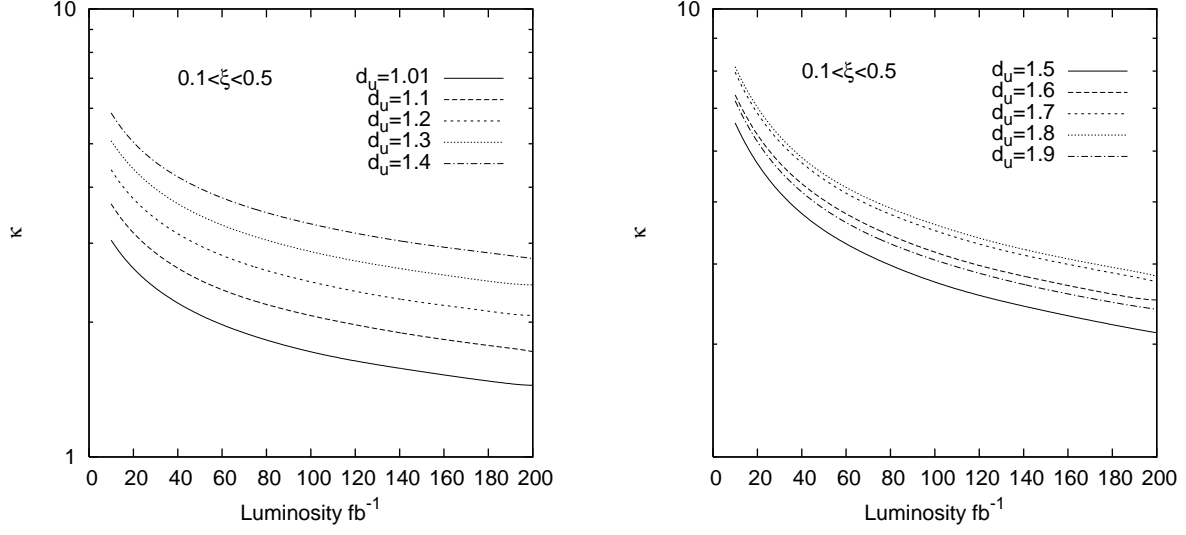


FIG. 15: 95% C.L sensitivity of  $pp \rightarrow p\gamma\gamma p$  to scalar unparticle coupling  $\kappa$  as a function of integrated LHC luminosity for an acceptance of  $0.1 < \xi < 0.5$ . Various values of the scale dimension are stated on the figures. We impose the cuts;  $|\vec{q}_{1t} + \vec{q}_{2t}| < 30\text{MeV}$  and  $|\eta| < 2.5$ .  $\Lambda_U$  is taken to be 3 TeV.

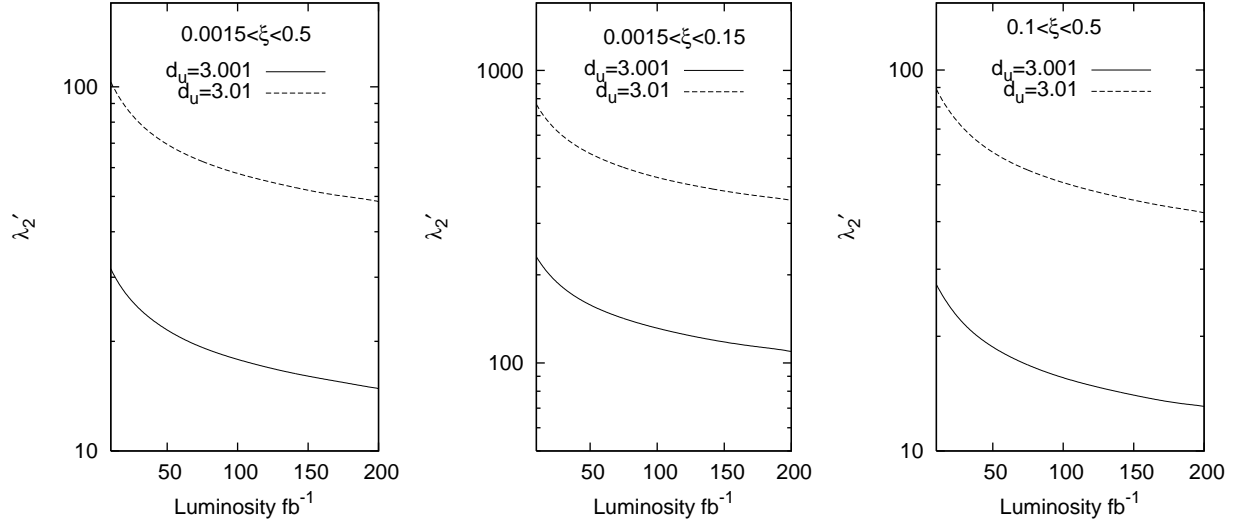


FIG. 16: 95% C.L sensitivity of  $pp \rightarrow p\gamma\gamma p$  to tensor unparticle coupling  $\lambda'_2$  as a function of integrated LHC luminosity. Different panels show different detector acceptances. The solid lines are for scale dimension  $d_U = 3.001$  and dotted lines are for  $d_U = 3.01$ . We impose the cuts;  $|\vec{q}_{1t} + \vec{q}_{2t}| < 30\text{MeV}$ ,  $\sqrt{s_{\gamma\gamma}} > 250\text{ GeV}$  and  $|\eta| < 0.88$  for the acceptances  $0.0015 < \xi < 0.5$  and  $0.0015 < \xi < 0.15$  and we impose  $|\vec{q}_{1t} + \vec{q}_{2t}| < 30\text{MeV}$  and  $|\eta| < 2.5$  for  $0.1 < \xi < 0.5$ .  $\Lambda_U$  is taken to be 3 TeV.

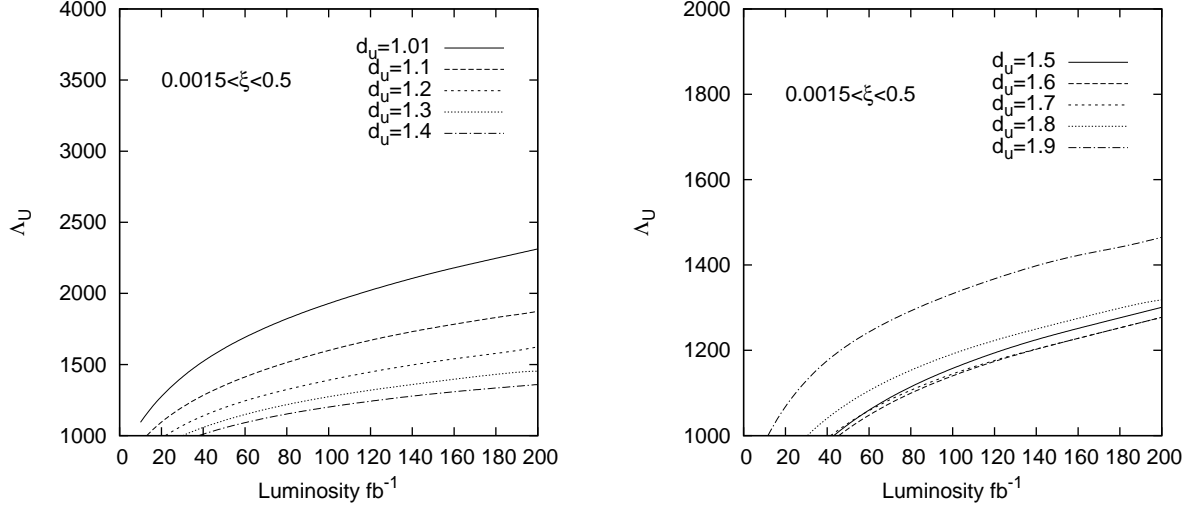


FIG. 17: 95% C.L. lower bounds on the energy scale  $\Lambda_U$  as a function of integrated LHC luminosity for  $pp \rightarrow p\gamma\gamma p$ . Various values of the scale dimension are stated on the figures. The couplings are taken to be  $\kappa=1$  and  $\lambda'_2 = 0$ . Limits of  $\Lambda_U$  are given in units of GeV. Forward detector acceptance is  $0.0015 < \xi < 0.5$  and we impose the cuts;  $|\vec{q}_{1t} + \vec{q}_{2t}| < 30\text{MeV}$ ,  $\sqrt{s_{\gamma\gamma}} > 250\text{ GeV}$  and  $|\eta| < 0.88$ .



TABLE I: Sensitivity of  $pp \rightarrow p\ell^-\ell^+p$  to the product of scalar unparticle couplings  $\kappa\lambda_S$  at 95% C.L. for various values of the scale dimension  $d_U$  and integrated LHC luminosities. We impose different cuts on the transverse momentum of final leptons for different luminosity values. Forward detector acceptance is  $0.0015 < \xi < 0.5$  and  $\Lambda_U$  is taken to be 3 TeV.

Luminosity	$10fb^{-1}$	$50fb^{-1}$	$100fb^{-1}$	$200fb^{-1}$
$p_{t,min}$	210 GeV	320 GeV	380 GeV	460 GeV
$d_U = 1.01$	(-1.4, 1.4)	(-1.0, 1.0)	(-0.8, 0.8)	(-0.7, 0.7)
$d_U = 1.1$	(-2.5, 2.5)	(-1.6, 1.6)	(-1.4, 1.4)	(-1.2, 1.2)
$d_U = 1.2$	(-4.8, 4.8)	(-2.9, 2.9)	(-2.3, 2.3)	(-2.0, 2.0)
$d_U = 1.3$	(-8.8, 8.8)	(-5.0, 5.0)	(-3.9, 3.9)	(-3.2, 3.2)
$d_U = 1.4$	(-15.6, 15.6)	(-8.1, 8.1)	(-6.4, 6.4)	(-5.2, 5.2)
$d_U = 1.5$	(-25.6, 25.6)	(-13.1, 13.1)	(-10.0, 10.0)	(-7.8, 7.8)
$d_U = 1.6$	(-40.6, 40.6)	(-19.7, 19.7)	(-15.0, 15.0)	(-11.3, 11.3)
$d_U = 1.7$	(-56.9, 56.9)	(-27.5, 27.5)	(-19.7, 19.7)	(-15.2, 15.2)
$d_U = 1.8$	(-67.8, 67.8)	(-32.5, 32.5)	(-23.4, 23.4)	(-17.3, 17.3)
$d_U = 1.9$	(-61.3, 61.3)	(-27.5, 27.5)	(-20.2, 20.2)	(-14.8, 14.8)

TABLE II: The same as table I but for  $0.0015 < \xi < 0.15$ .

Luminosity	$10fb^{-1}$	$50fb^{-1}$	$100fb^{-1}$	$200fb^{-1}$
$p_{t,min}$	200 GeV	310 GeV	360 GeV	420 GeV
$d_U = 1.01$	(-1.5, 1.5)	(-1.1, 1.1)	(-1.0, 1.0)	(-0.9, 0.9)
$d_U = 1.1$	(-2.7, 2.7)	(-2.0, 2.0)	(-1.6, 1.6)	(-1.5, 1.5)
$d_U = 1.2$	(-5.3, 5.3)	(-3.6, 3.6)	(-3.0, 3.0)	(-2.6, 2.6)
$d_U = 1.3$	(-10.0, 10.0)	(-6.4, 6.4)	(-5.3, 5.3)	(-4.4, 4.4)
$d_U = 1.4$	(-18.8, 18.8)	(-11.3, 11.3)	(-9.1, 9.1)	(-7.6, 7.6)
$d_U = 1.5$	(-33.8, 33.8)	(-19.4, 19.4)	(-15.6, 15.6)	(-12.7, 12.7)
$d_U = 1.6$	(-57.5, 57.5)	(-31.3, 31.3)	(-25.0, 25.0)	(-19.8, 19.8)
$d_U = 1.7$	(-90.6, 90.6)	(-47.5, 47.5)	(-37.5, 37.5)	(-29.3, 29.3)
$d_U = 1.8$	(-122.5, 122.5)	(-65.0, 65.0)	(-48.8, 48.8)	(-39.1, 39.1)
$d_U = 1.9$	(-122.5, 122.5)	(-62.5, 62.5)	(-48.7, 48.7)	(-37.1, 37.1)

TABLE III: Sensitivity of  $pp \rightarrow p\ell^-\ell^+p$  to  $\Lambda_U$  at 95% C.L. for various values of the scale dimension  $d_U$  and integrated LHC luminosities. We impose different cuts on the transverse momentum of final leptons for different luminosity values. The couplings are taken to be  $\kappa=\lambda_S=1$  and  $\lambda_{PS} = \lambda_2 = \lambda'_2 = 0$ . Lower bounds of  $\Lambda_U$  are given in units of GeV. Forward detector acceptance is  $0.0015 < \xi < 0.5$ .

Luminosity	$10fb^{-1}$	$50fb^{-1}$	$100fb^{-1}$	$200fb^{-1}$
$p_{t,min}$	210 GeV	320 GeV	380 GeV	460 GeV
$d_U = 1.01$	2109	3125	3625	4063
$d_U = 1.1$	1367	2000	2375	2625
$d_U = 1.2$	977	1406	1625	1875
$d_U = 1.3$	781	1094	1281	1438
$d_U = 1.4$	654	922	1063	1219
$d_U = 1.5$	596	828	953	1063
$d_U = 1.6$	557	773	875	1000
$d_U = 1.7$	557	758	859	969
$d_U = 1.8$	586	789	891	1000
$d_U = 1.9$	693	914	1031	1141

TABLE IV: The same as table III but for  $0.0015 < \xi < 0.15$ .

Luminosity	$10fb^{-1}$	$50fb^{-1}$	$100fb^{-1}$	$200fb^{-1}$
$p_{t,min}$	200 GeV	310 GeV	360 GeV	420 GeV
$d_U = 1.01$	2063	2734	3125	3469
$d_U = 1.1$	1313	1734	1992	2203
$d_U = 1.2$	906	1219	1367	1547
$d_U = 1.3$	703	938	1063	1172
$d_U = 1.4$	594	773	875	969
$d_U = 1.5$	516	680	766	844
$d_U = 1.6$	477	625	703	766
$d_U = 1.7$	461	594	664	734
$d_U = 1.8$	469	609	670	739
$d_U = 1.9$	533	680	750	825